Charge instabilities and phase separation in three-band extended Hubbard models: Effect of O-O hopping

N. Kothekar, K. F. Quader, and D. W. Allender
Department of Physics, Kent State University, Kent, Ohio 44224
(Received 14 July 1994)

We explore the interplay between various interaction and hopping terms, in particular the effect of O-O hopping, t_{pp}^{o} on the charge instabilities and phase separation in the three-band extended Hubbard models. Within a weak-coupling mean-field approach, we find that in two dimensions (2D), t_{pp}^{o} moves the phase separation boundary appreciably to higher dopings. This would increase the window of doping over which charge-transfer-mediated superconductivity can occur. Considering a larger phase space, we also obtain a more complete picture of the coexistence lines and spinodal decompositions, and determine the charge-transfer-instability critical point. We also consider the 1D case: t_{pp}^{o} is found to play a similar role, but the phase separation occurs at significantly lower dopings compared to 2D. This may be of interest to recent Monte Carlo calculations.

I. INTRODUCTION

In trying to arrive at a clear understanding of the instabilities of a system, it is natural to ask about the nature of incipient phase transitions, and whether the system would be in homogeneous or in coexisting phases. This is especially important for constructing a meaningful phase diagram of a system with competing instabilities. Generally, if two phases of a system have different symmetry, they are completely separated by a line of transitions, as for liquid and solid. The situation is different if there is no change in symmetry between the phases, as in the liquid and the gas phases in a Van der Waals fluid. As is well-known the first-order phase transition from the liquid to the gas phase ends in a critical point, as may be seen, for instance, on a pressure-temperature (p-T) phase diagram.[1] It is evident from the corresponding pressure-molar volume (p-V) diagram that a part of the p-V phase space is physically disallowed. In this region, instead of a single phase with a well-defined molar volume, the system separates into two coexisting phases with different molar volumes. The physical isotherm is then obtained by enforcing thermal and mechanical equilibrium. While in general it is not *a priori* clear if a system will undergo phase separation, it is expected if there is a first-order transition. Our study here will be concerned with an analogous situation that can arise in the extended Hubbard model for correlated electron systems.

In recent years there has been a tremendous interest in understanding the instabilities that may exist in correlated electron systems. Interacting electrons in solids are sufficiently screened from each other so that the underlying Coulomb interactions are often approximated by a shorter-range interaction. Accordingly, some variant of the Hubbard-Anderson models[2] with on-site interaction is expected to contain the key physics of correlated electron systems such as the transition metal oxides, high-T_c cuprates, etc.

With the discovery[3] of the high-T_c copper oxides, the study of Hubbard-like models have intensified greatly. The high-T_c cuprates exhibit diverse behavior as a function of doping: insulating, antiferromagnetic, metallic, superconducting, and possibly novel non-Fermi-liquid features.[4] A significant theoretical effort has been devoted to modeling the CuO_2 layers that form the basic building blocks of the cuprates. A large fraction of these calculations are within the framework of the two-dimensional (2D) *single-band* Hubbard model for on-site repulsion on Cu, or within the t-J model.[5] While these models have had a fair amount of success with the magnetic properties, especially at $\frac{1}{2}$-filling, they do not account for charge fluctuations on the same footing as spin excitations. Moreover, since the cuprates are low-density and essentially 2D systems, they are expected to be less screened than in usual 3D solids, so that the underlying interaction may be long-ranged. The *three-band* extended Hubbard model has been proposed[6,7] as a minimal model for describing the physical properties of these systems. Due to the presence of both intrasite and intersite interactions, the extended Hubbard model lends itself to a rich variety of competing instabilities and phase transitions. In special limits this model reduces to the t-J model or to the single-band Hubbard model.

The importance of nearest-neighbor Cu-O repulsion and on-site repulsion on Cu and O sites, for various charge and spin collective modes and instabilities, have been investigated both in the weak-[8–13] and strong-coupling[15,14,16] limits. Weak-coupling RPA calculations[11–13] have shown that a strong nearest-neighbor repulsion is important for different *charge instabilities* of the model. As we discuss later, for fairly large dopings the dominant instabilities are known[11] to be the charge transfer (CTI) and valence (VI) instabilities, which are driven by interband coupling induced by Cu-O interactions. It has also been suggested[6] that for Cu-O compounds, where the Cu and O orbital energies are close to each other, and the nearest-neighbor repulsion between them exceeds the Cu-O hybridization, extended s-wave or

0163-1829/95/51(9)/5899(9)/$06.00

d-wave pairing may be enhanced close to the charge-transfer instability. Subsequent detailed BCS (Ref. 8) and strong-coupling Eliashberg calculations[12] have shown that the interband charge-transfer resonance (CTR) or exciton can mediate an extended s-wave pairing with high transition temperatures. Strong-coupling ($1/N$ expansion) calculations[16] in the same model have since pointed out that the CTI is necessarily accompanied by a diverging uniform compressibility of the system. Then the pairing mediated by the CTR could be preempted by the occurrence of a charge phase separation in the region of doping where the pairing with the highest T_c's had been found earlier.[12] Subsequent weak-coupling mean-field (Hartree-Fock) calculations[17] are in agreement with this result. However, it is important to note that the effect of O-O *hopping* has not been taken into account in previous calculations. In addition, it is difficult to make quantitative comparisons since the collective boson used in the pairing calculations was obtained from a detailed RPA calculation on a lattice, and hence went beyond the static Hartree-Fock approximation.

In this paper, we carry out a detailed analysis of the charge instabilities of the three-band extended Hubbard model within a weak-coupling mean-field approach and reexamine the issue of charge phase separation. Thus we extend previous work[17] and study the interplay of various interaction and hopping kinetic-energy parameters. In particular, we examine carefully the effect of O-O *hopping* on the *charge phase separation.* In so doing, we have attempted to provide a physical understanding of phase separation in this model by drawing analogy with the phenomenon in other systems. We find that the model exhibits a first-order transition line of valence instability (at constant density), ending in a "critical point." As in the case without O-O hopping, we also find a locus of charge-transfer instability (at constant chemical potential), that coincides with the line of divergent compressibility. In agreement with previous findings,[16,17] we find that the system separates into coexisting phases with different valences, i.e., different Cu and O occupancies. The phase-separation boundary surrounds both the VI critical point as well as the line of CTI. But one of the main points we want to make here is the significant role that O-O hopping plays in determining the location of the instabilities and the region of phase separation. This is important to the question of pairing via charge excitations. The phase-separation boundary is shifted by an appreciable amount to larger dopings, away from the regime where superconductivity was obtained in earlier calculations.[8,11,12] This is to be contrasted with previous weak-coupling results.[17]

We also explore a larger parameter space than previously studied so as to examine more completely the region of phase separation, and the spinodal lines. This enables us to locate the CTI *critical point,* distinct from the VI critical point. We comment on the possible dynamics of the nonequilibrium phenomena to be expected from such a model system at dopings in the phase-separation region.

In addition to the two-dimensional case in Sec. II, we also consider the *one-dimensional* extended Hubbard model in Sec. III. The findings are similar to that in 2D, except all the phenomena occur at a substantially lower doping. This may be of interest to recent Monte Carlo calculations of pairing in 1D.[18]

II. STUDY OF THE 2D CASE

A. Extended Hubbard model and mean-field approximation

We begin with the Hamiltonian for the 2D extended Hubbard model defined for the $d_{x^2-y^2}$ orbital on Cu and the p_x and p_y orbitals on the corresponding two O atoms in the unit cell (Fig. 1 shows a unit cell in the copper-oxide layer):

$$H=\sum_{\langle i,j\rangle,\sigma} t_{ij}^{o}(d_{i\sigma}^{\dagger}p_{j\sigma}^{x,y}+\text{H.c.})+\epsilon_d^0\sum_{i,\sigma} d_{i\sigma}^{\dagger}d_{i\sigma}+\epsilon_p^o\sum_{j,\sigma}(p_{j\sigma}^{x\dagger}p_{j\sigma}^{x}+p_{j\sigma}^{y\dagger}p_{j\sigma}^{y})+t_{pp}^{o}\sum_{\langle j,j'\rangle,\sigma\sigma'}(p_{j\sigma}^{x\dagger}p_{j'\sigma'}^{y}+\text{H.c.})+U_d\sum_i(n_{d_{i\uparrow}})(n_{d_{i\downarrow}})$$
$$+U_p\sum_j[(n_{p_{j\uparrow}}^{x})(n_{p_{j\downarrow}})^{x}+(n_{p_{j\uparrow}}^{y})(n_{p_{j\downarrow}}^{y})]+V\sum_{\langle i,j\rangle,\sigma\sigma'} n_{d_{i\sigma}}n_{p_{j\sigma'}}\,. \tag{1}$$

The vacuum is taken to be the usual $d^{10}p^6$ configuration. Thus the $d_{i\sigma}^{\dagger}$ ($d_{i\sigma}$) operators are the creation (annihilation) operators for holes in the $d_{x^2-y^2}$ orbitals of Cu atoms while $p_{\sigma}^{x\dagger}$ and $p_{\sigma}^{y\dagger}$ are the corresponding operators for the p_x and p_y orbitals on the O site. σ is a spin index and $\langle i,j\rangle$ is the nearest-neighbor sum; ϵ_p^o and ϵ_d^o are the atomic levels on O and Cu, respectively; the occupation numbers per spin, $n_{d_{i\sigma}}=d_{i\sigma}^{\dagger}d_{i\sigma}$ and $n_p^{x,y}=p_{j\sigma}^{\dagger x,y}p_{j\sigma}$. t_{ij}^{o} is the Cu-O hybridization energy and corresponds to the overlap of the Cu and O orbitals. As can be seen from Fig. 1, the difference in symmetry between the Cu d and O p orbital is such that t_{ij}^{o}, which corresponds to the overlap integral of Cu and O orbitals, takes the values $\pm t_{pd}^{o}$ alternately within a layer. Also included in H are the on-site repulsions U_d and U_p for holes on Cu and O sites, respectively, and the repulsion V between nearest-neighbor holes on the Cu and O sites. Finally, t_{pp}^{o} represents the oxygen p_x-p_y hybridization energy and causes hole hopping between the two nearest-neighbor oxygen sites. As we shall show, the inclusion of t_{pp}^{o} is very important for the location of the instabilities and phase separation in this model.

In order to obtain the band structure for the model, we Fourier transform the Hamiltonian in the usual way by introducing Wannier functions. Diagonalization of the noninteracting part of H in the Wannier basis yields the usual tight-binding bands: antibonding (AB) band, bonding (B) band, and a mixed band. In the absence of t_{pp}^{o}, the

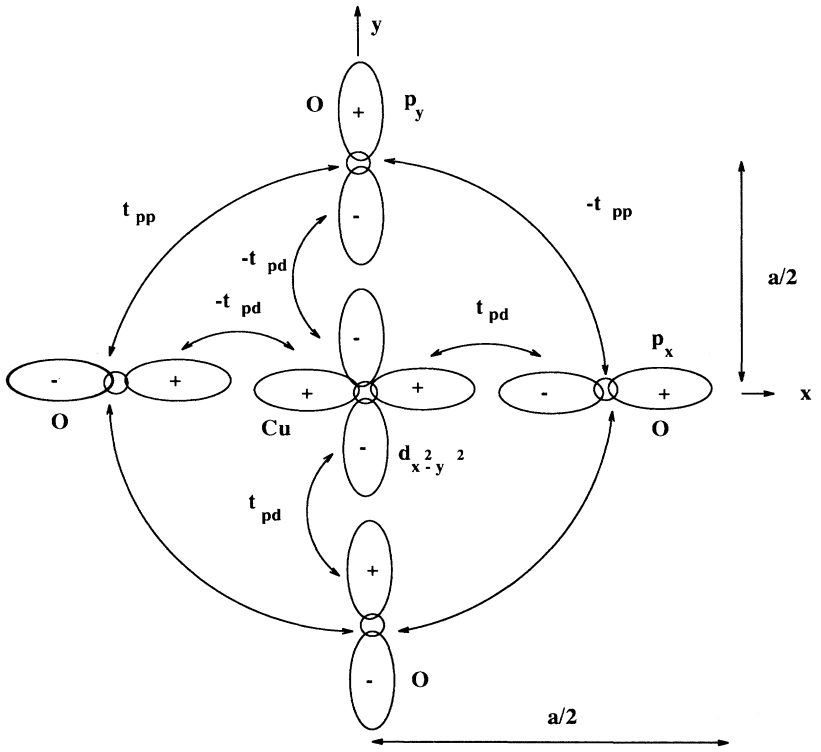

FIG. 1. Schematic diagram of a unit cell in the Cu-oxide layer showing the orbitals, their symmetries, and the hybridizations t_{pp} and t_{pd}. a is the distance between any two neighboring Cu or O sites.

mixed band reduces to the usual flat nonbonding (NB) band. The eigenvalues corresponding to the three bands are

$$\lambda_i=\frac{1}{3}\left\{2\alpha\cos\left[\sin^{-1}\left[\frac{\beta}{2\alpha^3}\right]\Big/3+g_i\right]+\frac{\epsilon_o}{2}\right\}, \tag{2}$$

where $\alpha=\sqrt{(3a+3bt_{pp}^o+\epsilon_o^2)}$, and

$$\beta=-9a\epsilon_o-2\epsilon_o^3-9b(-2t_{pp}^o\epsilon_o+6t_{pd}^{o2}),$$

with

$$a=4t_{pd}^{o2}[\sin^2(k_xa/2)+\sin^2(k_ya/2)],$$

and

$$b=16t_{pp}^o\sin^2(k_xa/2)\sin^2(k_ya/2),$$

$$g_i=-\pi/6,\pi/2,-5\pi/6,$$

respectively, for AB, mixed, and B bands. $\epsilon_o=\epsilon_p^o-\epsilon_d^o$ denotes the energy difference between the O p level and the Cu d level in the absence of any interaction. The oxygen level lies higher than the copper level, and the reference level is chosen such that $\epsilon_p^o=\epsilon^o/2=-\epsilon_d^o$. The first Brillouin zone is defined by $|k_{x,y}|\le\pi/a$.

As in Ref. 17, we work in the hole picture, i.e., within the lowest-lying bonding band; the insulating half-filled state then corresponds to one hole per unit cell. In this scheme, inclusion of the interaction terms in the Hamiltonian renormalizes the orbital energies ϵ_p^o and ϵ_d^o, and the p-d hybridization energy t_{pd}^o. The renormalized energies can be obtained by minimizing $\langle H\rangle$ among a class of variational wave functions $|\psi(\epsilon,t_{pd},t_{pp}^o)\rangle$ where $|\psi\rangle$ is the ground state of the noninteracting part of the Hamiltonian with renormalized ϵ_o and t_{pd}^o.[9] For the bonding band ($\lambda=\lambda_3$), the resulting variational wave function is

$$|\psi^o(\epsilon^o,t_{pd}^o,t_{pp}^o)\rangle=\prod_{k,\sigma}(u_kd_{k\sigma}^\dagger+v_kp_{k\sigma}^{x\dagger}+w_kp_{k\sigma}^{y\dagger})|0\rangle \tag{3}$$

with $u_ku_k^*+v_kv_k^*+w_kw_k^*=1$, and u_k, v_k, and w_k to be determined. An equivalent approach to direct minimization of energy is to linearize the interaction terms in the Hamiltonian by making the Hartree-Fock approximation and then calculating the number densities self-consistently. This entails replacing two of the four-fermion operators, i.e., products of the type $a^\dagger a$ by their averages $\langle a^\dagger a\rangle$. Only the expectation values that conserve hole numbers survive. All others average to zero.

The mean-field "self-consistency" equations can then be shown to be

$$\epsilon=\epsilon_p-\epsilon_d=\epsilon^o+\left[\frac{U_p}{4}-\frac{U_d}{2}\right]\frac{1+\delta}{2}+4\left[V-\frac{U_d}{8}-\frac{U_p}{16}\right](\langle n_d\rangle-\langle n_p\rangle) \tag{4}$$

and

$$2it_{pd}=2it_{pd}^o+V(\langle p_x^\dagger d\rangle-\langle p_y^\dagger d\rangle), \tag{5}$$

where $\langle n_d\rangle=\sum_k u_ku_k^*$; $\langle n_p\rangle=\frac{1}{2}(\langle n_p^x\rangle+\langle n_p^y\rangle)$ with $\langle n_p^x\rangle=\sum_k v_kv_k^*$ and $\langle n_p^y\rangle=\sum_k w_kw_k^*$; and

$$\langle d^\dagger p_{x,y}\rangle=1/N\sum_{k'}\sin(k'_{x,y}a/2)u_{k'}^*\gamma_{k'},$$

where $\gamma_{k'}=v_{k'}(w_{k'})$ for the $p_x(p_y)$ orbitals; δ is the hole doping, and $(1+\delta)/2=\langle n_d\rangle+\langle n_p\rangle$ is the total hole density. All the energies are in units of t_{pd}^o. It is important to note that the O-O hopping t_{pp}^o manifests itself in the expectation values $\langle n_d\rangle$, $\langle n_p\rangle$, $\langle d^\dagger p_{x,y}\rangle$, etc.

B. Charge instabilities

The *renormalized* Cu-O energy difference $\epsilon=\epsilon_p-\epsilon_d$ controls the valence of the system. This together with the renormalized bandwidth t_{pd}, and the O-O hopping t_{pp}^o are important for studying the instabilities of the model. t_{pp}^o is not renormalized since the Hamiltonian does not explicitly contain an interaction term for the repulsion between the nearest-neighbor oxygen, i.e., an interaction of the type V_{pp}.

On solving numerically the mean-field self-consistency equations [Eqs. (4) and (5)], as in Ref. 17, we find that the renormalized level ϵ may not necessarily be a single-valued nor a continuous function of the parameters. For a fixed V, U_p, U_d, ϵ_o, and t_{pp}^o, with increasing doping δ, the valence becomes unstable, i.e., ϵ jumps discontinuously to a negative value. This discontinuous jump could alternatively be seen on a plot of ϵ vs ϵ^o, wherein the jump appears as ϵ^o is reduced at fixed doping (Fig. 2). The jump in ϵ is associated with an abrupt change in the relative occupancy of Cu and O orbitals. This has been termed[11,17] *valence instability,* VI. At this point the valence susceptibility, defined as the charge-transfer susceptibility (CTS) at *constant density* and given by

$$\chi_\delta\equiv\left.\frac{\partial(n_p-n_d)}{\partial\epsilon^o}\right|_\delta, \tag{6}$$

diverges.

Some of the features of VI have been discussed previously.[16,17] Here we shall focus on the effect of O-O hopping. Its effect is to push the VI to higher dopings. This is shown in Fig. 3(a) for a representative value of $t_{pp}=0.2$. The location of VI, δ_{VI} shows signs of flattening as t_{pp}^o is increased to values of $t_{pp}^o\approx 0.35$ [Fig. 3(b)]. The O-O hopping also tends to act counter to the effect of V, the nearest-neighbor repulsion between Cu and O. In the absence of t_{pp}^o, increasing V pushes the system towards the VI instability at lower dopings. Consequently, at a fixed hole density, for a nonzero t_{pp}^o, a larger V is needed to drive the model to the instability at the same doping; see Fig. 4. Thus the role of t_{pp}^o is similar to that of U_d and opposite to that of V.

The collected mode associated with VI has the full A_{1g} symmetry of the underlying lattice.[11] Hence the VI line, obtained from examining the instability at different dop-

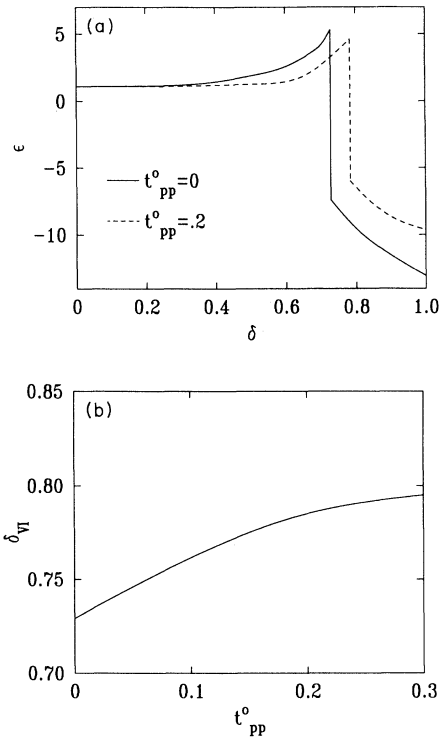

FIG. 3. (a) Effect of O-O hopping (t_{pp}^o). Shown is the variation of ϵ with doping δ. The discontinuity in ϵ moves to higher dopings as t_{pp}^o is increased. $V=2.5$, $U_d=3$, $U_p=1$, and $\epsilon_o=1.1$. (b) Position of the discontinuity in ϵ as a function of t_{pp}^o. The figure shows how this discontinuity saturates for low values of t_{pp}^o in the 2D case.

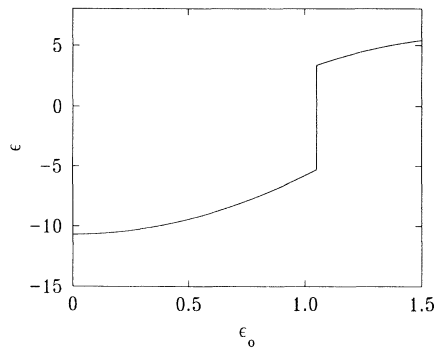

FIG. 2. Discontinuous jump in ϵ as ϵ_o is varied at a fixed doping ($\delta=0.7$). $V=2.5$, $U_d=3$, $U_p=1$, and $t_{pp}^o=0.2$.

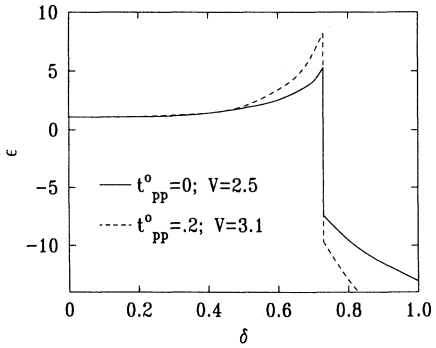

FIG. 4. Effect of V in the presence of t_{pp}^o. $U_d=3$, $U_p=1$, and $\epsilon_o=1.1$. The system becomes unstable at a higher V in the presence of t_{pp}^o.

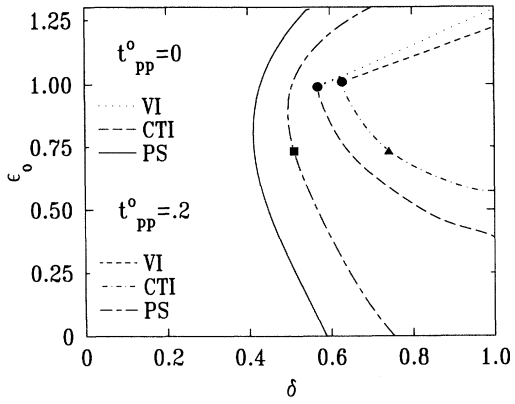

FIG. 5. Phase diagram for the 2D model in the ϵ_o-δ plane for $V=2.5$, $U_d=3$, $U_p=1$, and $\epsilon_o=1.1$ for $t^o_{pp}=0$ and 0.2. Shown are the valence instability (VI) lines ending in critical points, the CTI lines, and the phase-separation (PS) lines for both values of t^o_{pp}. The points marked by the square and the triangle correspond to the points on Fig. 8 and are obtained from Maxwell's construction.

ings, δ, is not expected to be symmetry breaking, and the transition is necessarily first order. The VI line is shown in the ϵ^o-δ plane in Fig. 5; it ends in a "critical point" $(\epsilon^o_{\rm VI}, \delta_{\rm VI})$. At the VI line ϵ, obtained from the mean-field equations [Eqs. (4) and (5)] is multivalued; the solution that minimizes the free energy has been chosen to be the physical one. In Fig. 5, moving across the VI line in ϵ^o, at a fixed doping, the valence ϵ jumps discontinuously, as shown in Fig. 6. If ϵ^o is reduced beyond the VI critical point, the valence becomes a continuous function of doping, as also shown in Fig. 6. Comparison of the VI lines for $t^o_{pp}=0$ and 0.2 in Fig. 5 shows that it is moved to higher dopings by a nonzero O-O hopping.

To appreciate related instabilities in the system, it may be observed that although the VI line is not symmetry breaking, an appropriately constructed free energy should contain coupling to all degrees of freedom having the same symmetry, as well as to $n_{\rm tot}$. Following Littlewood,[19] the fluctuating part of the free energy, expanded about the equilibrium may be written as

$$
\begin{aligned}
F &= F[\delta(n_p-n_d),\delta n_{\rm tot}] \\
&= \tfrac{1}{2}\chi_\delta^{-1}(\delta n_p-\delta n_d)^2 \\
&\quad -\epsilon^o(\delta n_p-\delta n_d)+\tfrac{1}{2}\kappa^{-1}\delta n_{\rm tot}^2 \\
&\quad -\mu\delta n_{\rm tot}+\alpha(\delta n_p-\delta n_d)\delta n_{\rm tot}, \qquad (7)
\end{aligned}
$$

where

$$
\chi_\delta = \left.\frac{\partial^2 E}{\partial(n_p-n_d)^2}\right|_n^{-1} = \frac{\partial(n_p-n_d)}{\partial\epsilon^o}
$$

is the previously defined valence susceptibility or the CTS at constant density; μ is the chemical potential, κ the compressibility in the absence of coupling to charge transfer, and α a coupling constant. As one approaches the VI critical point, χ_δ diverges. But due to coupling, the instability of the model can occur when CTS at a *constant chemical potential* (χ_μ) diverges, i.e.,

$$
\chi_\mu|^{-1}=\chi_\delta|^{-1}-\alpha^2\kappa\to 0\ . \qquad (8)
$$

This divergence of χ_μ, termed charge-transfer instability, is accompanied by the divergence of the uniform compressibility, $\kappa=dn_{\rm tot}/d\mu$. The locus of such points on the phase diagram (Fig. 5) defines the metastable spinodal line along which χ_μ and the uniform compressibility diverge simultaneously. This had been arrived at by a different argument in previous work[16,17] that did not include t^o_{pp}. In addition to the VI lines, Fig. 5 also shows the CTI lines for t^o_{pp} of 0 and 0.2. It is evident that t^o_{pp} moves CTI to higher dopings as well.

C. Phase separation

The issue of the accompanying *phase separation* can be readily understood on considering the behavior of μ with δ.[17] As shown in Fig. 7, the behavior of μ with respect to δ is similar to that of ϵ; it becomes continuous beyond the VI critical point. In the continuous region, the divergence of χ_μ can be obtained by looking for dopings where $d\mu/dn_{\rm tot}=0$, i.e., where the compressibility diverges. Figure 7 shows that beyond the discontinuity in μ or beyond the point at which $d\mu/dn_{\rm tot}=0$ (for the dashed

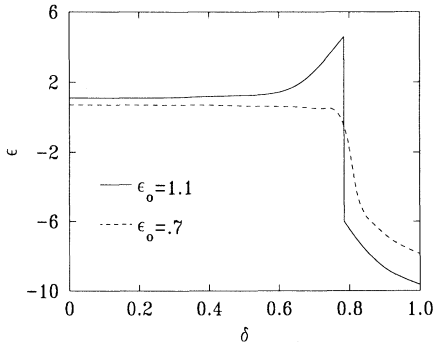

FIG. 6. Variation of ϵ as a function of δ for two values of ϵ_o. The figure shows the discontinuity in ϵ disappearing as the critical point is crossed. Here $V=2.5$, $U_d=3$, $U_p=1$, and $t^o_{pp}=0.2$.

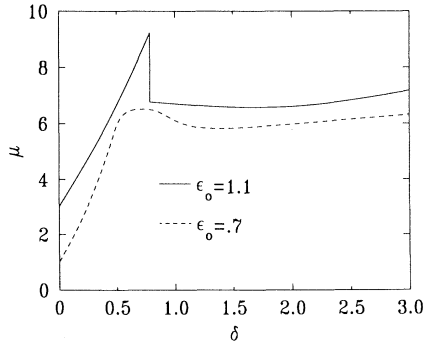

FIG. 7. Variation of chemical potential with doping for $V=2.5$, $U_d=3$, $U_p=1$, and $t^o_{pp}=0.2$. The discontinuity in μ disappears as the critical point is crossed.

curve), the chemical potential *decreases* with increasing doping. The compressibility is thus negative and signals a charge phase separation in the model. This is reminiscent of the case of a Van der Waal's fluid.[1] There in the p-V plane, the isotherms exhibit *nonanalytic* behavior at the boundaries of the two-phase (liquid and gas) region. But as an artifact of the Van der Waal's equations being *analytic* throughout the two-phase region, the liquid phase is continued into the region of the phase diagram where it is in fact metastable or even unstable. In other words, the isothermal compressibility, $\kappa_T = -1/V(dV/dp)_T < 0$. This is because global equilibrium conditions had not been ensured from the outset. The horizontal physical isotherm is properly constructed by enforcing thermal and mechanical equilibrium, which is tantamount to performing a Maxwell equal area construction in the p-V plane. Analogously, here a region of μ-δ phase space is disallowed, and the corresponding Maxwell construction has to be carried out in the μ-δ plane. This is shown in Fig. 8 for a set of parameters. A and B represent the two equal areas. The triangles represent the points at which the compressibility diverges, whereas the squares denote the lower limit of the unphysical part of the μ vs δ curve, and thus lie on the phase separation line. These are shown on the phase diagram, Fig. 5.

Insight into the model in general may be gained by examining a more complete phase space. For this, though, the numerical values of ϵ_o and δ has to be extended to ranges that are unrealistic for the cuprates. This is shown in Fig. 9 for $t_{pp}^o = 0.2$. Here the $t_{pp}^o \neq 0$ part of the phase diagram from Fig. 5 is repeated showing both the charge-transfer instability and the valence instability, including the VI critical point (solid circle) at lower doping. In addition, the large-δ part of the phase-separation diagram is also shown. It should be noted that in this region we find the CTI critical point, distinct from the VI critical point; this is indicated by the solid square at $(\delta = \delta_c = 1.96,\ \epsilon = \epsilon_0^c = -1.317)$, so that at $\epsilon_o < \epsilon_o^c$, no phase separation occurs. For $\epsilon_o > \epsilon_o^c$, the solid lines indicate the two states that form as phase separation occurs. The dashed lines are spinodal lines since the regions between the solid and dashed lines are metastable: these states have higher energy than the phase-separated states, but still have a positive compressibility. The region enclosed by the dashed lines is completely unstable (i.e., the compressibility is negative). Note that at large ϵ_o, this unstable region collapses, and the first-order VI line (also shown in Fig. 9) divides the two metastable regions. An example showing the consequence of the phase separation may be found by choosing a fixed $\epsilon_o = 0.4$. A system doped so that $\delta_1 = 0.596 < \delta < \delta_2 = 2.265$ will separate into inhomogeneous configuration where some regions have δ_1 and others δ_2. The relative volumes of the sample having δ_1 and δ_2 are such that the average doping is δ. The actual configuration that results will be determined by the dynamics of the phase separation and the interfacial surface energy considerations.

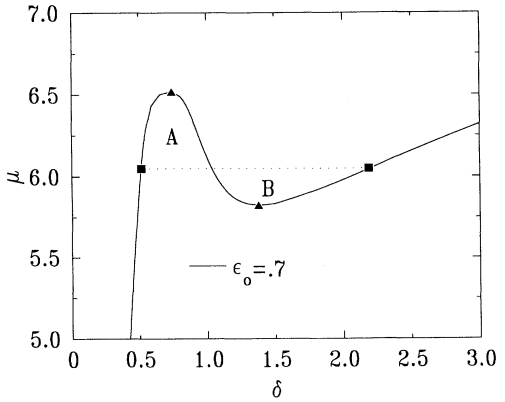

FIG. 8. Maxwell's construction in the μ-δ plane. $V = 2.5$, $U_d = 3$, $U_p = 1$, and $t_{pp}^o = 0.2$. A and B represent the two equal areas. The triangles mark the points where the compressibility diverges and the squares denote the boundary of the unstable part of the μ vs δ curve.

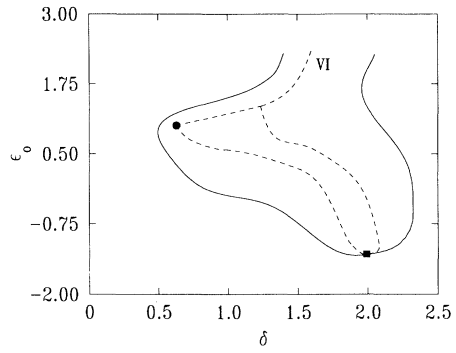

FIG. 9. A more complete picture of phase separation in the 2D extended Hubbard model. The parameters are those of Fig. 5, and $t_{pp}^o = 0.2$. The solid lines represent the phase-separation boundary, ending at the CTI critical point ($\delta_c = 1.96$, $\epsilon_o^c = -1.317$), denoted by the solid square. The dashed lines are the metastable spinodal lines. The first-order VI line that divides two metastable regions is indicated by "VI;" it ends in the VI critical point ($\delta_{VI} = 0.63$, $\epsilon_{VI} = 1.01$), shown as a solid circle.

In is instructive to compare the phase-separation (PS) line for a *nonzero* O-O hopping with that for $t_{pp}^o = 0$. As evident from Fig. 5, the PS boundary moves by an appreciable amount to higher dopings for a modest $t_{pp}^o = 0.2$. Generally, the phase separation, as well as the charge instabilities of the model, are found to be very sensitive to O-O hopping. As opposed to V that promotes charge segregation, including t_{pp}^o in the model promotes charge uniformity. Earlier calculations,[17] that did *not* include O-O hopping, found that in the weak-coupling limit, the extended s-wave pairing region lies within the thermodynamically disallowed region. To properly compare with these results, we use the same set of parameters used in those calculations, and reconstruct the phase diagram shown in Fig. 10. We find that, as in our previous case (Fig. 5), the PS boundary is moved to higher densities even in the presence of a modest t_{pp}^o. This increases the window of doping over which charge-transfer-mediated superconductivity can occur, and in fact the pairing region is found to lie well *outside* the region of phase separation. It must however be pointed out that the superconductivity calculations[12] were done using the random-

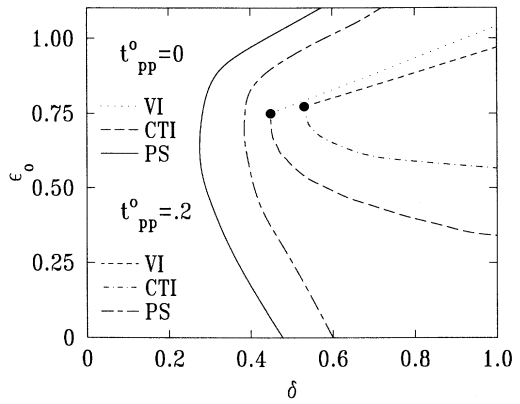

FIG. 10. Phase diagram for the 2D case for $t^o_{pp}=0$ and 0.2, for another set of parameters, namely $V=1.8$, $U_d=2$, and $U_p=0$.

phase approximation (RPA) and thus true comparison between the two results is difficult. On the other hand, it is known that pairing mediated by interband charge-transfer excitation is *comparatively* more robust to the variation of parameters such as t^o_{pp}.[11,20] The point we would like to make here is that O-O hopping appears to play an important role in the issue of phase separation, and has to be properly accounted for. By contrast, it appears not to be crucial for pairing. This may be roughly understood as follows: One of the chief effects of different hopping terms is to modify the shape of the Fermi surface in ways that do not have an appreciable effect on pairing, which is more susceptible to changes in interactions. On the other hand, introduction of additional near-neighbor hopping makes it energetically favorable for the holes to progress from an inhomogeneous configuration to a more homogeneous one, thus inhibiting phase separation. Thus hopping kinetic energy has a more significant effect on short-range phenomena such as charge instabilities and phase separation than on long-range order such as superconductivity. In view of the sensitivity of perturbative calculations to model parameters such as O-O hopping, we feel that one has to be cautious in arriving at conclusions regarding competing instabilities and coexisting phases.

III. STUDY OF THE 1D CASE

For the sake of completeness, and owing to current interest,[18,21] we also studied phase separation in the 1D extended Hubbard model. For instance, our calculation would be of relevance to recent 1D calculation of the pairing instability by Monte Carlo methods.[18] O-O hopping in the 1D case comes into play in a slightly different manner than in 2D. In this case we consider a chain of alternating Cu and O atoms, say along the x axis. Thus, t^o_{pp} in the 1D model corresponds to hopping between the two nearest oxygen sites, i.e., $p_x - p_x$. Such an interaction term was ignored in the 2D case since we were interested only in the leading O-O hopping term which corresponds to hopping between the p_x-p_y orbitals of O.

The Hartree-Fock Hamiltonian for the 1D problem reduces to

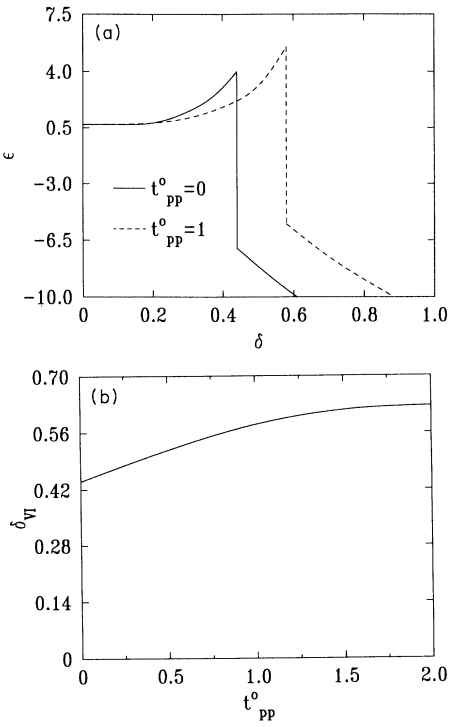

FIG. 11. (a) Effect of t^o_{pp} in 1D. Here $V=1.8$, $U_d=3$, $U_p=1$, and $\epsilon^o=0.7$. (b) Position of the discontinuity as a function of t^o_{pp}.

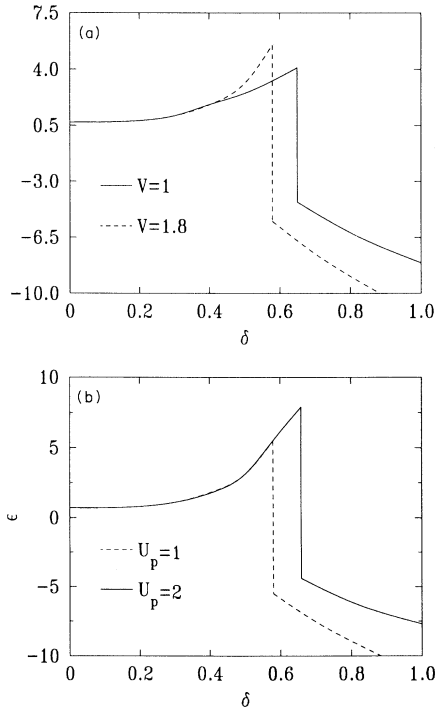

FIG. 12. (a) Effect of V in 1D. $U_d=3$, $U_p=1$, $\epsilon^o=0.7$ and $t^o_{pp}=1$. (b) Effect of U_p in 1D. $V=1.8$.

$$H=\sum_{k,\sigma}[\epsilon_d^o d_{k,\sigma}^\dagger d_{k,\sigma}+\epsilon_p^o p_{k,\sigma}^\dagger p_{k,\sigma}]+\sum_{k,\sigma}2it_{pd}^o[\sin(ka/2)d_{k,\sigma}^\dagger p_{k,\sigma}-\sin(ka/2)p_{k,\sigma}^\dagger d_{k,\sigma}]$$
$$+\sum_{k,\sigma}2t_{pp}^o\cos(ka)p_{k,\sigma}^\dagger p_{k,\sigma}+U_d\langle n_d\rangle\sum_{k,\sigma}d_{k,\sigma}^\dagger d_{k,\sigma}+U_p\langle n_p\rangle\sum_{k,\sigma}p_{k,\sigma}^\dagger p_{k,\sigma}$$
$$+4V\sum_{k,\sigma}[n_d d_{k,\sigma}^\dagger d_{k,\sigma}+n_p p_{k,\sigma}^\dagger p_{k,\sigma}]-2V\sum_{k,\sigma}[\langle d^\dagger p\rangle p_{k,\sigma}^\dagger d_{k,\sigma}\langle p^\dagger d\rangle d_{k,\sigma}^\dagger P_{k,\sigma}]\sin(ka/2)\,, \tag{9}$$

where $\langle n_{d,p}\rangle$ and $\langle p^\dagger d\rangle$ are the 1D analogs of the corresponding averages in 2D, and can be obtained in analytic forms. The noninteracting part of H gives rise to two tight-binding bands with energies that depend on t_{pp}^o. As in the 2D case, here also we work with the lower band. The above equations need to be solved self-consistently. The mean-field equations in the 1D case are

$$\epsilon=\epsilon^o-U_d n_d+U_p n_p-4V(n_p-n_d)\,,$$
$$t_{pd}=t_{pd}^o+2V\langle p^\dagger d\rangle\,. \tag{10}$$

The results of our calculations for the 1D model are similar to those obtained in 2D. However, since in 1D, each Cu is surrounded by only two oxygen compared to four in the 2D case, the effect of O-O hopping is expected to be relatively more pronounced. Consequently, the flattening of the VI instability is reached at a much higher doping in the 1D model [Figs. 11(a) and 11(b)]. The effects of V and U_p on charge instability are similar to those found in the 2D model [Figs. 12(a) and 12(b)]. Thus in both 1D and 2D, at a fixed doping, V promotes instability whereas U_p moves the system towards equilibrium. Figure 13 shows a typical phase diagram for the 1D case. Although qualitatively similar to the 2D results, even in the presence of a fairly large $t_{pp}^o\approx 1.0$, the PS boundary occurs at significantly lower dopings. Thus, it is conceivable that phase separation may compete with possible pairing transition in 1D; recent Monte Carlo calculations.[18] find pairing to occur quite close to half-filling. We note that in talking about pairing instabilities in lower dimensions, we have taken the liberty of making the usual tacit assumption that fluctuations are stabilized by some weak couplings in other dimensions.

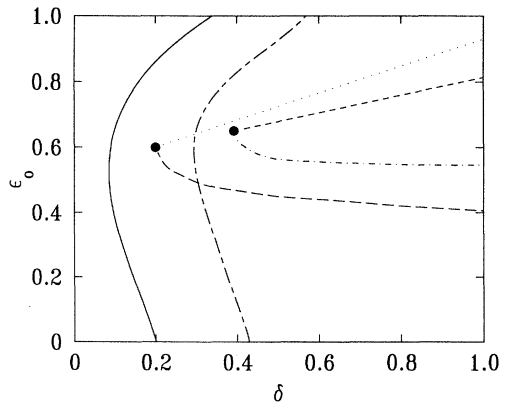

FIG. 13. Phase diagram for the 1D case. Here $V=1.8$, $U_d=3$, and $U_p=1$. The figure shows two cases, namely, $t_{pp}^o=0$ and 1.0.

IV. CONCLUSIONS

In conclusion, our main results are as follows.

(a) We have investigated the role of O-O hopping and its interplay with other model parameters both in the 2D and the 1D extended Hubbard models. We have studied the effects on the instabilities and consequently on phase separation in these two cases. We have found that the charge instabilities, as well as the phase separation are quite sensitive to O-O hopping. In the 2D case, this increases the window of parameter space over which pairing can occur.

(b) To gain further insight into the charge instabilities and phases of the two-dimensional case, we have extended our calculation into a larger parameter space. Part of this parameter range is unphysical for the cuprates, nevertheless may be of interest more generally. This allowed us to obtain the CTI critical point, the complete boundaries of phase separation, and the spinodal decompositions at both the lower and higher doping regions of the phase space.

We remark that the occurrence of phase separation in these types of models is presumably due to the short-range nature of the interactions in the Hamiltonian. In the presence of truly long-range forces as the Coulomb interaction, phase separation will be suppressed, unless compensated by screening charges. One may still be able to see charge phase separation on a short length scale, giving rise to some sort of "striped phases." But this will depend on the competition between the long-range Coulomb force and the fluctuating part of the free energy. It would be interesting to explore this possibility.

ACKNOWLEDGMENTS

We would like to thank Peter Littlewood for several discussions, suggestions, and encouragement during the

course of this work. We also thank Y. Bang, D. Johnson, G. Kotliar, and S. Trugman for various comments and their help. This work was partially supported by grants from the KSU Research Council and NASA Grant No. NCC 3-222. One of us (K.F.Q.) acknowledges the hospitability of the Center for Materials Science and the T-11 division at Los Alamos National Laboratory, where part of this work was completed.

[1]Herbert B. Callen, *Thermodynamics and an Introduction to Thermostatistics* (Wiley, New York, 1985), p. 233.
[2]J. Hubbard, Proc. R. Soc. London Ser. A **276**, 238 (1963); P. W. Anderson, Phys. Rev. **115**, 2 (1959).
[3]J. G. Bednorz and K. A. Müller, Z. Phys. B **64**, 189 (1986).
[4]P. W. Anderson, Science **235**, 1196 (1987); E. Abrahams, in *Advances in Superconductivity II, ISS '89,* Tsukuba, Japan, edited by T. Ishiguro and K. Kajimura (Springer-Verlag, New York, 1990), p. 7.
[5]F. C. Zhang and T. M. Rice, Phys. Rev. B **36**, 381 (1977).
[6]C. M. Varma *et al.*, Solid State Commun. **62**, 681 (1987); in *Novel Mechanisms of Superconductivity,* edited by V. Kresin and S. Wolf (Plenum, New York, 1987), p. 355.
[7]V. J. Emergy, Phys. Rev. Lett. **58**, 2794 (1987).
[8]P. B. Littlewood, C. M. Varma, and E. Abrahams, Phys. Rev. Lett. **63**, 2602 (1989).
[9]S. N. Coppersmith and P. B. Littlewood, Phys. Rev. B **41**, 2641 (1990).
[10]P. B. Littlewood, C. M. Varma, S. Schmitt-Rink, and E. Abrahams, Phys. Rev. B **39**, 12 371 (1990).
[11]P. B. Littlewood, Phys. Rev. B **42**, 10 075 (1990).
[12]Y. Bang, K. Quader, E. Abrahams, and P. B. Littlewood, Phys. Rev. B **42**, 4865 (1990).
[13]R. Putz, G. Dopf, B. Ehlers, L. Lilly, A. Muramatsu, and W. Hanke, Phys. Rev. B **41**, 853 (1990).
[14]S. A. Trugman, Phys. Scr. **T27**, 113 (1989).
[15]J. E. Hirsch, E. Loh, Jr., D. J. Scalapino, and S. Tang, Phys. Rev. B **39**, 243 (1989).
[16]M. Grilli *et al.*, Phys. Rev. Lett. **67**, 259 (1991); M. Grilli *et al.*, Phys. Rev. B **47**, 3323 (1993); **47**, 3331 (1993); M. Grilli, R. Raimondi, C. Castellani, C. Di Castro, and G. Kotliar, Int. J. Mod. Phys. B **5**, 309 (1991).
[17]Y. Bang, G. Kotliar, C. Castellani, M. Grilli, and R. Raimondi, Phys. Rev. B **43**, 13 724 (1991).
[18]E. Dagotto, J. Riera, Y. C. Chen, A. Moreo, A. Nazarenko, F. Alcaraz, and F. Ortolani, Phys. Rev. B **49**, 3548 (1994), and references therein.
[19]P. B. Littlewood, in *Correlated Electron Systems,* Jerusalem Winter School for Theoretical Physics, Vol. 9, edited by V. Emery (World Scientific, Singapore, 1993), p. 1.
[20]P. B. Littlewood (private communication).
[21]N. Andrei (private communication).